Theor Chem Acc (2006) 116: 670–682
DOI 10.1007/s00214-006-0113-5

REGULAR ARTICLE

Michael J. Bearpark · Martial Boggio-Pasqua
Michael A. Robb · François Ogliaro

Excited states of conjugated hydrocarbons using the molecular mechanics - valence bond (MMVB) method: conical intersections and dynamics

Received: 20 December 2004 / Accepted: 9 May 2005 / Published online: 21 February 2006

Abstract We developed the molecular mechanics—valence bond (MMVB) method following an original suggestion of Jean-Paul Malrieu and coworkers. By coupling a parameterized Heisenberg Hamiltonian to a standard classical force field (MM2), reliable ground and excited state geometries of conjugated hydrocarbons can be rapidly optimized. The MMVB method was central to our development of algorithms for locating conical intersections and calculating their associated decay dynamics. Here, we briefly review the chemical applications of MMVB to date, and present two new studies using the photostability of pyracylene and the excited state decay dynamics of the photochromic dihydroazulene/vinylheptafulvene (DHA/VHF) reaction.

Keywords Heisenberg Hamiltonian · Excited state calculations · Valence bond theory · Conjugated hydrocarbons · QM/MM

1 Introduction

We are very happy to be able to contribute this paper to a special issue recognizing the work of Jean-Paul Malrieu in quantum chemistry. Several suggestions of Jean-Paul and his coworkers have made a major impact on our own work, particularly the idea that valence bond (VB) theory is both a natural way to think about excited state reactivity [1–3] and a powerful technique for calculating excited state potential energy surfaces, once effective Heisenberg spin Hamiltonians are introduced [4–16]. Our implementation of this is the molecular mechanics–valence bond (MMVB) method [17,18], which has been employed in over twenty studies to date [19–40], and which was central to our development of algorithms for locating conical intersections [20] and calculating their associated decay dynamics [22,40]. As part of a long-term development plan for MMVB, we have now interfaced our code to the Gaussian [41] computational chemistry package.

The MMVB method is described in detail elsewhere [17,18,38,39]. The original aim [17] was to simulate complete active space self consistent field (CASSCF) calculations for the ground and excited states of conjugated hydrocarbons, and to generate starting points for CASSCF geometry optimizations. MMVB has now outgrown this limited aim, for which the geometries were more than good, because the calculated relative energies were often also surprisingly good [29] and thus the method was usable in its own right.

One way to appreciate how MMVB works is to recognize that a CASSCF wavefunction can be transformed into (i.e. projected onto [16,42]) a VB wavefunction via construction of an effective Hamiltonian [15]. Malrieu and coworkers recognized that the resulting VB integrals, Coulomb (Q) and exchange (K), had a simple distance and orientation dependence that could be fitted [9,10]. Our implementation [17] extended this original idea by fitting the exchange integrals additionally as a function of 'hybridization' (sp^2/sp^3), and also by recognizing that much of the total Coulomb energy can be provided by a standard molecular mechanics potential [14] (here MM2 [43]). The resulting MMVB method is many orders of magnitude faster than the CASSCF method it was designed to simulate, because expensive integral evaluation has been completely replaced by analytic fitted functions. There is still a Hamiltonian and hence an eigenvalue problem to solve, which means that MMVB can describe excited states and bond reorganization using an 'active space' of orbitals as in CASSCF. However, there is a significant speedup here too, as the VB representation scales much better with the number of active orbitals than CASSCF: for coronene [18] for example (24 active electrons), VB gives $\sim 3 \times 10^6$ Slater determinants for the ground S_0 state, instead of $\sim 1 \times 10^{12}$ with CASSCF. This is because the electron basis functions

M. J. Bearpark (✉) · M. Boggio-Pasqua · M. A. Robb
Chemistry Department, Imperial College,
South Kensington Campus,
London SW7 2AZ, UK
E-mail: m.bearpark@imperial.ac.uk

F. Ogliaro
Equipe de Chimie et Biochimie Théoriques—UMR 7565,
Université Henri Poincaré, Nancy 1, BP 239
54506 Vandoeuvre-lès-Nancy Cedex, France

with $S_z = 0$ where all of the orbitals are singly occupied (VB), are fewer compared to those where an orbital can be doubly or singly occupied, or unoccupied (CASSCF). The VB 'perfect-pairing' basis functions are therefore a small subset of those that would be used in CASSCF. Because of this, MMVB calculations can be carried out on molecules for which CASSCF calculations are currently impossible, even with high symmetry. But this has also meant so far a lack of optimized excited state geometries and non-vertical excitation energies against which to benchmark MMVB.

Molecular mechanics–valence bond currently has a number of disadvantages. The first is that parameters must be generated for elements with 'active' orbitals, and we currently implement only sp^2/sp^3 carbon atoms this way (although many different 'inactive' atoms can be treated via MM2, as in e.g. ergosterol [19]). We use a general set of parameters, not fitted for any particular molecule (although we have experimented with this [38]), which introduces some approximations. The extension to active orbitals on elements other than carbon [11,12] has not been so straightforward. In some ways we are fortunate that there are so many interesting conjugated hydrocarbons! To treat active orbitals on elements other than carbon, we have the problem that more than one active orbital per atom may be necessary (e.g. lone pairs for N/O). Also there is the restriction of the Heisenberg Hamiltonians used to 'valence' (covalent) excited states, a point well understood by Malrieu et al. [2]. However, this is also a limitation of CASSCF, unless the active space is extended (for e.g. ionic states [1,44]), resulting in more active orbitals than active electrons. Other QM/MM methods for treating excited states have been proposed, with different advantages and disadvantages, including [79–84].

One of the most successful early applications of the MMVB method was to the ultrafast radiationless decay of the azulene molecule [22]. The idea that conical intersections of ground and excited potential energy surfaces could be responsible for such decay and the accompanying lack of fluorescence was becoming more acceptable at that time. After reading about the problem in Turro's book [45], the initial MMVB calculations for azulene took less than a day to run, including location of the suspected accessible conical intersection (Fig. 1). However, the CASSCF calculations required to check these MMVB results took over 18 months, given the computer resources available to us at the time. It is very unlikely that these CASSCF calculations would have been attempted without the initial MMVB geometries.

Azulene is a paradigm for ultrafast radiationless decay, but also for photostability: because the crossing shown in Fig. 1 is sloped (S_1 and S_0 having similar gradients) [46], the most likely decay path on S_0 is back to the initial reactant and not on to form new products. In this paper, we present new calculations on the pyracylene molecule (Fig. 2), which is also known to be photostable and nonfluorescent [47]. Recognising Jean-Paul Malrieu's concern that quantum chemistry can be more about numbers than understanding [48], we find that the accessible conical intersection between the S_1 and S_0 states of pyracylene responsible for its photostability has

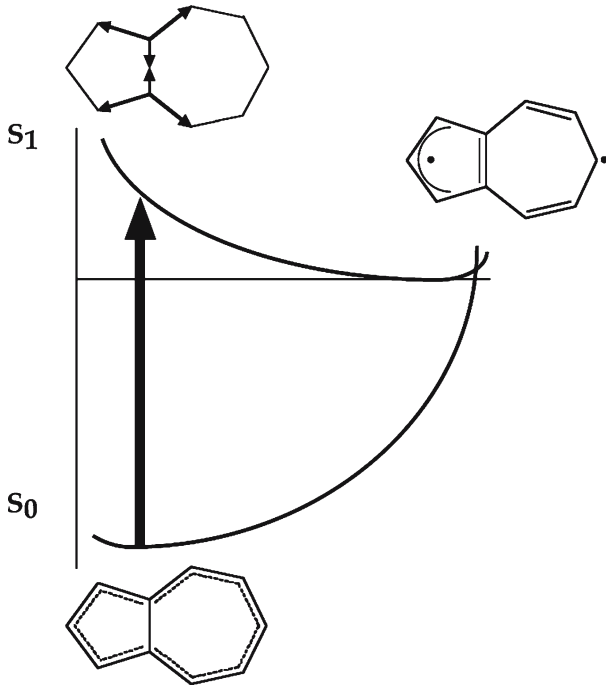

Fig. 1 The azulene S_1/S_0 conical intersection [22]: the S_0 and S_1 potential energy surfaces have minima at very different geometries, and relaxation on S_1 (indicated by *arrows top left*) leads to the sloped intersection, at which efficient radiationless decay occurs

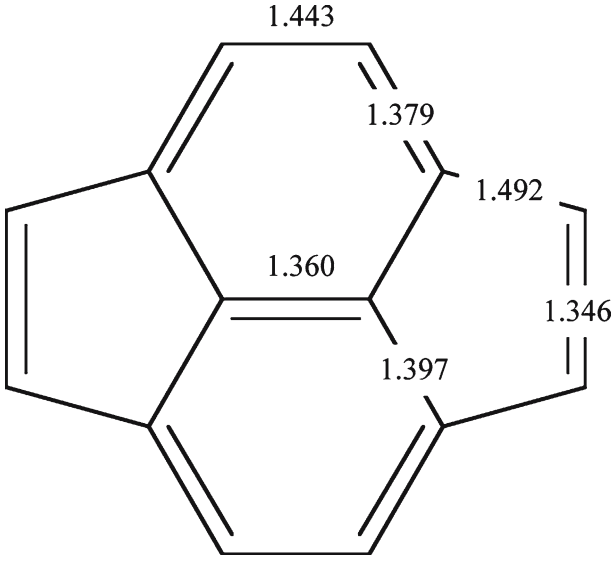

Fig. 2 The crystal structure of pyracylene [47], showing distinct single and double bond alternation. All bond lengths in Å

a similar origin to the crossing in azulene. The differences from azulene can be rationalized with VB theory [49].

Because MMVB is so much faster than CASSCF, we were able to run dynamics calculations to investigate decay in the azulene S_1/S_0 crossing region [22]. These were direct dynamics calculations (no fitted potential surfaces) with surface hopping; the codes were not originally designed with

sloped crossings in mind, and we now appreciate that recrossing and oscillatory population transfer are key features of decay in these regions. MMVB dynamics has also been used to calculate product distributions from a photochemical 4+4 cycloaddition [30] (where there are several distinct crossing regions between ground and excited states), soliton behavior in polyenes [2,35], and dynamical energy transfer between naphthalene and anthracene chromophores linked by a methylene bridge [34].

In this paper, we present an MMVB dynamics study of the related dihydroazulene/vinylheptafulvene (DHA/VHF) photochromic system [50–52] (Fig. 3). Here we faced some problems with our current MMVB parameterization, as the relative energies of several critical points in the crossing region of DHA/VHF are not quite right. Nevertheless, our dynamics results are consistent with the experimental result that DHA reacts photochemically to give VHF but that VHF is photostable. For azulene, the crossing is described as unavoidable because it is accessible along a reaction path that is in the same direction as the initial relaxation on the first excited state (Fig. 1), and this reaction path coincides with one of the two coordinates responsible for creating the degeneracy at the crossing, the branching space [46,53]. The azulene dynamics calculations showed that increasing kinetic energy could lead to decay at higher-energy regions of the crossing seam, but that decay in the region of the crossing minimum was still favored. In contrast, the excited state reaction path from DHA does not coincide with the branching space, and vibrations orthogonal to the reaction path therefore control decay (as discussed more fully in e.g. [40]). Our MMVB dynamics calculations show that from DHA, a different higher-energy region of the S_1/S_0 crossing seam is favored compared to VHF, where the initial relaxation direction leads to a region closer to the crossing minimum. Recent work [54,55] suggests that cases where the excited state reaction path does not lead directly to the crossing minimum will be common. Dynamics calculations are essential for even a qualitative mechanistic understanding of decay at these crossings, making extensions of MMVB-like methods for additional elements and electronic states highly desirable.

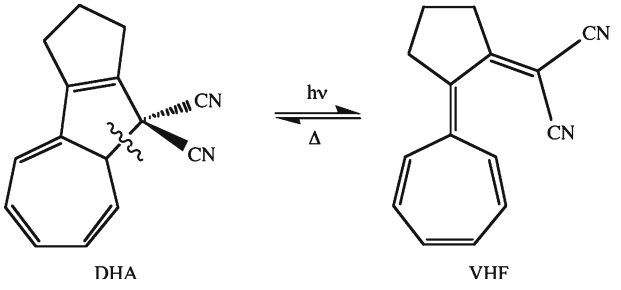

Fig. 3 The photochromic dihydroazulene/vinylheptafulvene (DHA/VHF) isomerisation [51,52]: DHA reacts to give VHF photochemically, whereas VHF is photostable and only reverts to DHA on heating

2 Computational methods

Molecular mechanics–valence bond [17,18] is a hybrid quantum / molecular mechanics (QM/MM) method, which currently uses the MM2 potential [43] to describe a sigma bonded molecular framework. The active electrons–those involved in conjugation or new sigma-bond formation–are represented by a Heisenberg Hamiltonian [15,16] in the space of neutral valence bond configurations. Because of this, the MMVB method can only treat covalent states at present, and the active sites are currently only parameterized for sp^2/sp^3 carbon atoms (although inactive sites within the sigma bonded framework can include any atom for which MM2 is defined). MMVB differs from many other QM/MM methods in that the quantum and molecular mechanics parts are both present on certain (hybrid) atoms, and not separated into different (hybrid) regions of a molecule. A VB carbon atom in MMVB has one free valence at present: some parameters in the potential for this atom were obtained from transformed CASSCF wavefunctions for model systems [38]; some others were modified from the standard MM2 force field. However, these modified parameters are interdependent, and geometry dependent. Sigma-pi separation is not enforced, and the interaction between sigma and pi electrons is treated at a similar level to CASSCF for the molecules studied here: the underlying sigma framework can adapt to reorganization of the pi system and is not fixed.

Using effective Hamiltonian theory, a CASSCF wave function with localized active orbitals can be projected onto the space of neutral valence-only VB structures [16] and interpreted as a Heisenberg Hamiltonian [6,9,16]. Heisenberg-like VB Hamiltonians are particularly suitable for parameterization, because of the distance and orientation dependence of their matrix elements Q_{ij} and K_{ij} (like those in the Heitler-London VB treatment of the H_2 molecule [56]). This leads to formulae which are evaluated analytically in MMVB [17], and hence there is none of the integral evaluation, orbital optimization or state-averaging necessary with CASSCF. Q_{ij} and K_{ij} in MMVB are independent of the particular electronic state being optimized.

Molecular mechanics–valence bond can describe the formation of new sigma bonds from p orbitals in a π system. However, we encountered some problems here with our current parameterization of the terms in the Heisenberg Hamiltonian needed to describe new sigma bond formation, specifically, the behavior of the formulae for determining Q_{ij} at long range (>2.5 Å). To try to minimize the problem, we included only the Q_{ij} terms necessary to describe the sigma bond that is broken or formed (Fig. 3). However, DHA structures (with this sigma bond ~1.5 Å) are consequently much too low in energy relative to VHF structures on a particular potential energy surface. The same set of MM and VB connections need to be used for a molecule if the relative energies of different structures are to be compared.

For dynamics calculations, the MMVB energy and gradient are used to solve the Newtonian equations of motion. Details of our implementation have been given elsewhere

[21]. This is a 'direct' dynamics method: the trajectories are propagated using a series of local quadratic approximations to the MMVB potential energy surface, as suggested by Helgaker et al. [57], with the step size determined by a trust radius [58]. The surface-hopping algorithm of Tully and Preston [59, 60] is used to allow excited state trajectories to transfer to the ground state in the conical intersection region. Surface hopping is sufficiently accurate for our purpose here in showing that decay can take place at a realistic crossing geometry (see e.g. [85] for a discussion of some of the problems with this approach). Other methods for treating transfer between electronic states exist, including Ehrenfest dynamics (e.g. with MMVB [31] and subsequently [86]), spawning [87,88] and variational Gaussian wavepackets [89].

The sampling of the nuclear positions and momenta was generated in different ways, depending on where the trajectories were started for DHA/VHF. A reference trajectory (trajectory 0) was started from the VHF ground state geometry on S_1 without any initial kinetic energy. For the rest of the VHF trajectories, the initial S_1 geometries and velocities were sampled on S_0 at the same geometry, using the S_0 vibrational modes. On the DHA side, all of the trajectories were started in the region of the S_1 transition structure. A reference trajectory (trajectory 0) was computed, with an initial kinetic (translational) energy of 2 kcal mol^{-1} along the transition vector from the S_1 TS pointing towards the photoproduct (VHF). For the other DHA trajectories, the same excitation of the transition vector was applied as for the reference trajectory, and a thermal sampling of 300 K was generated in the remaining S_1 vibrational modes on the S_1 potential energy surface. More details about the sampling can be found in reference [61]. For pyracylene, only one trajectory was computed, sampling all of the ground state vibrational modes at the $D_{2h}S_0$ minimum.

Molecular mechanics–valence bond energies and geometries were compared with the results of ab initio calculations. For the CASSCF calculations on pyracylene, we used MOLPRO [62] to take advantage of point group symmetry (D_{2h}/C_{2h}). So far, the largest active space used to benchmark MMVB against CASSCF included 13 active electrons/orbitals for the phenalenyl radical (D_{3h}) [39]. There, reasonable agreement was obtained with geometries to within ± 0.02 Å, and excitation/relaxation energies to within a few kcal mol^{-1}. We have occasionally seen disagreement between MMVB and CASSCF when there are several low-lying excited states [32], which is why benchmarks on real systems are important for the future development of the MMVB method. CASSCF calculations were run using the 4–31G basis set, as this was the basis set used to parameterize MMVB originally [17]. For DHA/VHF, we compared our MMVB results with previously published CASSCF calculations [52]. MMVB calculations were run using a development version of the Gaussian code [41].

The CASSCF calculations for pyracylene were performed by distributing 14π electrons in the 14π orbitals, generating around 690,000 configurations in D_{2h} symmetry and 1,380,000 in C_{2h}. Optimizing a conical intersection using MOLPRO with such a large active space is currently too expensive, so we used the restricted active space self consistent field (RASSCF) method, reducing the number of configurations by restricting the excitations in the wavefunction. This reduction is done by subdividing the active space into three categories: a set of orbitals with a limited number of vacancies (called the RAS1 space), a fully active orbital set (RAS2), and a set of orbitals with a limited number of electrons (RAS3). We limited the excitations from the RAS1 space to singles and doubles only, and allowed at most two electrons in RAS3. To obtain reliable results, we had to calibrate the RASSCF S_0–S_1 energy gap in the region of the crossing against the CASSCF value. We computed this energy gap at the optimized MMVB conical intersection geometry, where the degeneracy of the two states is lifted by 8.2 kcal mol^{-1} with CASSCF. We used all 14 π electrons in the RASSCF calculations, and the size of the RAS2 space was progressively increased until the $S_0 - S_1$ energy gap became acceptable (error below 1 kcal mol^{-1}) at this geometry. The least expensive RASSCF calculation that was performed used two active orbitals in RAS2 (the HOMO and LUMO orbitals necessary to describe the first two excited states), for which the computed S_0–S_1 energy gap was 11.4 kcal mol^{-1}. We then enlarged RAS2 and shrank RAS1 and RAS3 so that the orbitals with the largest occupation numbers were left in RAS1 and the orbitals with the lowest occupation numbers were kept in RAS3. Using four active orbitals in RAS2, the S_0–S_1 energy gap is reduced to 7.0 kcal mol^{-1}. Using six orbitals in RAS2 brings the energy gap to 7.8 kcal mol^{-1}, just 0.4 kcal mol^{-1} away from the target CASSCF value. The number of configurations is then around 48,000, which makes the optimization of the S_1/S_0 crossing possible.

3 Results and discussion: pyracylene

The X-ray structure of pyracylene [47] (Fig. 2) was found to have D_{2h} symmetry, with pronounced alternation of single and double bond lengths [63], particularly in the 5-membered rings (1.35, 1.49 Å).

Fig. 4 shows the corresponding $D_{2h}S_0$ minimum for pyracylene obtained with MMVB. All bond lengths are reproduced to within ± 0.02 Å apart from the etheno bridges fused to the naphthalene fragment, which are 1.44 Å in the crystal structure and 1.47 Å with MMVB. Both CASSCF (14,14)/4–31G and B3LYP/6–31G* calculations [63] give 1.45 Å for the same bond length; closer to the crystal structure (Fig. 2) than MMVB. All computational methods reproduce the pattern of single/double bond alternation determined experimentally.

With MMVB, we also calculate a shallow imaginary frequency for out-of-plane distortion of this D_{2h} structure on S_0 (Fig. 4). Because the energy change is ~ 0.001 kcal mol^{-1} and a B3LYP/6–31G* frequency calculation does not give any negative frequencies, we have treated the $D_{2h}S_0$ minimum as the real S_0 minimum with MMVB in what follows.

The 0–0 S_1 transition of pyracylene was measured at $\sim$650 nm/44 kcal mol^{-1} [47]. Radiationless deactivation of

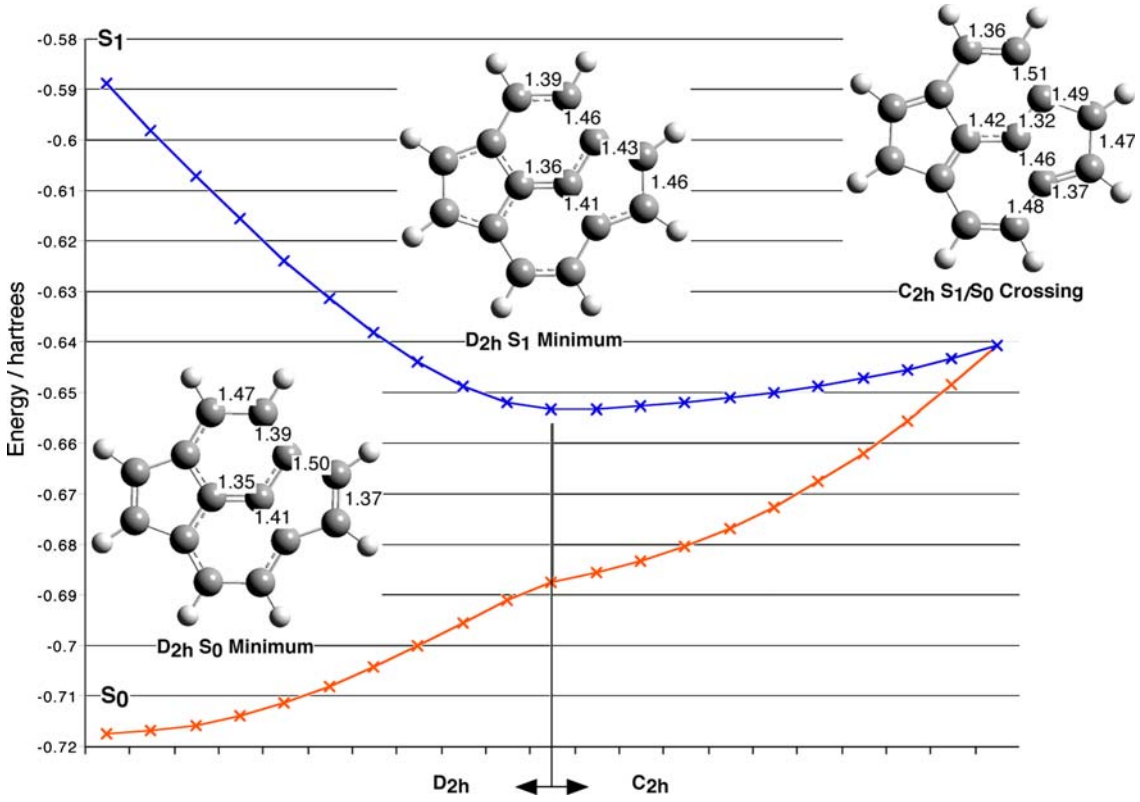

Fig. 4 Molecular mechanics–valence bond (MMVB) linear interpolation from the S_1 Franck-Condon geometry ($S_0\,D_{2h}$ minimum) to the $S_1\,D_{2h}$ minimum, and then to the C_{2h} real crossing minimum. All bond lengths in Å

Table 1 Molecular mechanics – valence bond (MMVB) energies for pyracylene (Figs. 2, 4)

Structure	State	*E*/hartrees	*E* on S_0/kcal mol^{-1}	*E* on S_1/kcal mol^{-1}	$\Delta E(S_1–S_0)$/kcal mol^{-1}
S_0 minimum	S_0	−0.71731	0.000		
D_{2h}	S_1	−0.58862		40.550	80.754
S_1 minimum	S_0	−0.68728	18.844		
D_{2h}	S_1	−0.65324		0.000	21.360
S_1/S_0 crossing	S_0	−0.64080	48.011		
C_{2h}	S_1	−0.64073		7.850	0.044
S_1/S_0 crossing	S_0	−0.63519	51.530		
D_{2h}	S_1	−0.62240		19.351	8.026
S_0 isomer	S_0	−0.69400	14.627		
D_{2h}	S_1	−0.60356		31.175	56.752

the lowest excited singlet state was very rapid, and no fluorescence was detectable. Vibrational fine structure in the absorption spectrum was more pronounced in glassy alkane solution at 77 K, but the S_0–S_1 absorption remained diffuse. Rapid radiationless deactivation, lack of fluorescence and diffuse absorption spectra are all 'symptoms' of an accessible conical intersection on the excited state. Furthermore, no photochemical reactions were detected and pyracylene was described as photostable [47], both of which suggest that the conical intersection is sloped [46], as in azulene [22] (Fig. 1).

Fig. 4 shows the S_1 minimum and S_1/S_0 crossing minimum located with MMVB. The calculated 0–0 energy of 40 kcal mol^{-1} (from Table 1) is only slightly less than the experimental value of 44 kcal mol^{-1}. The MMVB S_1 minimum has D_{2h} symmetry: the central five C–C bonds are unchanged compared with the S_0 minimum, but there is a complete inversion of bond lengths in the perimeter [64]. Because of this difference in character of the S_1 and S_0 states, it follows that there is a considerable relaxation energy on S_1, and the S_1 minimum is $\sim$ 40 kcal mol^{-1} below the Franck-Condon geometry. In addition, the energy gap between S_1 and S_0 is already reduced to $\sim$20 kcal mol^{-1} at the $D_{2h}S_1$ minimum (Table 1).

Unexpectedly, the minimum located on the S_1/S_0 conical intersection seam for pyracylene has C_{2h} symmetry (Fig. 4). Table 1 shows that the crossing is $\sim$8 kcal mol^{-1} above the S_1 minimum, well below the vertically excited geometry and therefore energetically accessible.

Attempts to optimize a D_{2h} crossing were unsuccessful: Fig. 5 (left) shows that the smallest energy gap found

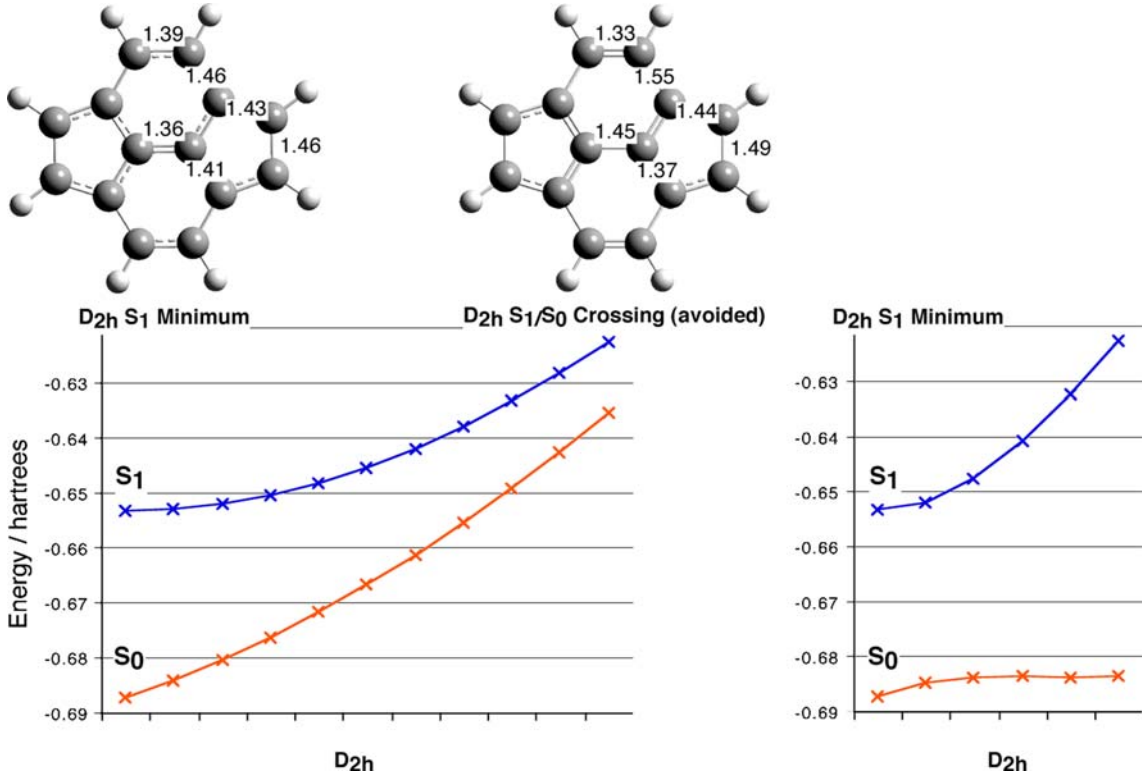

Fig. 5 *Left* MMVB linear interpolation from the S_1 D_{2h} minimum to a D_{2h} avoided crossing. *Right* a continuation of the D_{2h} coordinate which leads from the Franck-Condon geometry to the S_1 D_{2h} minimum (Fig. 4), continuing beyond the S_1 minimum, showing that the S_1 and S_0 states diverge. NB: *left and right figures* show interpolations along different D_{2h} coordinates. All bond lengths in Å

was 8 kcal mol^{-1}, at the point labeled $D_{2h}S_1/S_0$ crossing (avoided). Linear interpolation from the $D_{2h}S_1$ minimum to this point shows that the S_1 and S_0 states are brought together slowly. Fig. 5 (right) shows a linear interpolation from the $D_{2h}S_1$ minimum along a distinctly different D_{2h} coordinate: the coordinate that leads from the Franck-Condon geometry on S_1 to the $D_{2h}S_1$ minimum. Continuing along this coordinate beyond the $D_{2h}S_1$ minimum as shown in Fig. 5 (right), leads to the S_1 and S_0 states diverging, with the S_1 state steeply rising in energy. Contrasting Fig. 5 (right) with Fig. 4 (right hand side) suggests that two equivalent C_{2h} decay pathways leading to conical intersections emerge from the $D_{2h}S_1$ minimum, and that decay is unlikely to take place at D_{2h} geometries on S_1.

We can rationalize why the pyracylene S_1/S_0 crossing has C_{2h} symmetry and not D_{2h} symmetry by comparison with azulene. For azulene (Fig. 1), the VB electronic structure at the crossing shows a localized allyl radical and another distant unpaired electron, and it is these four weakly coupled electrons which must be accommodated to make the two states degenerate [49,65,66]. For pyracylene in D_{2h} symmetry, there is no way to obtain a comparable electronic structure without lowering the symmetry to C_{2h}, for in D_{2h}, there are no perimeter carbon atoms on any of the C_2 symmetry axes.

No benzene-like crossings were found (where one carbon atom has been lifted out-of-plane [21,67]) despite extensive searching. All attempts to displace one of the perimeter carbons out of plane and optimize a crossing led back to the planar $C_{2h}S_1/S_0$ crossing structure (Fig. 4).

The linear interpolation shown in Fig. 4 suggests that the C_{2h} conical intersection is sloped and that the gradients on the S_1 and S_0 potential energy surfaces are approximately parallel, resembling azulene (Fig. 1). The coordinates that lift the degeneracy at this crossing to first order (derivative coupling and gradient difference vectors; the branching space) are shown in Fig. 6. The reaction path that leads from the D_{2h} minimum on S_1 to the C_{2h} crossing (Fig. 4) is dominated by the gradient difference vector (UGD), and this reaction path therefore lies in the branching space, suggesting that decay in the region of the lowest energy point on the crossing will be favored.

The MMVB results suggest that the C_{2h} crossing is energetically accessible, because the energy required to reach the crossing is less than the vibrational excess energy available on S_1 after relaxation from the Franck-Condon geometry (Table 1). However, the reaction path leading to the crossing (C_{2h}) changes direction [61] from the initial relaxation direction (D_{2h}). To test whether decay at the C_{2h} crossing is likely to occur, dynamics calculations were run starting from the Franck Condon geometry on S_1. Even though the crossing does not lie along the D_{2h} relaxation coordinate leading from Franck-Condon structure to the S_1 minimum (cf. azulene, Fig. 1), the crossing is still accessible. Fig. 7 shows an MMVB trajectory that hops from S_1 to S_0, with a crossing

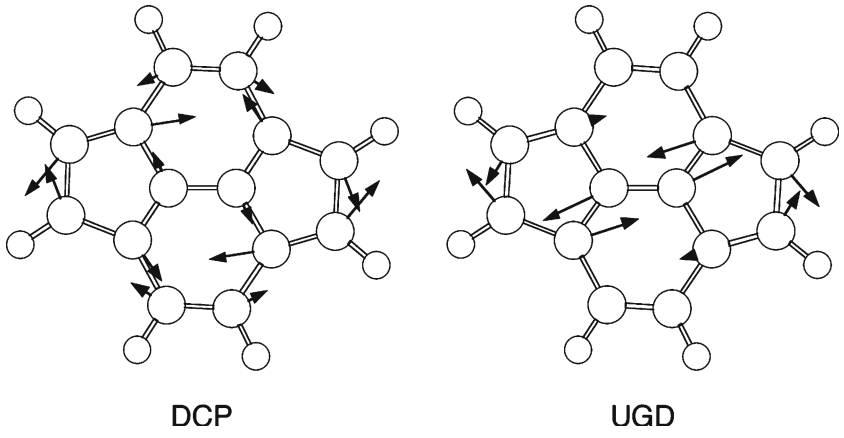

Fig. 6 Derivative coupling (DCP) and gradient difference (UGD) vectors, which lift the degeneracy to first order, at the C_{2h} S_1/S_0 crossing shown in Fig. 4

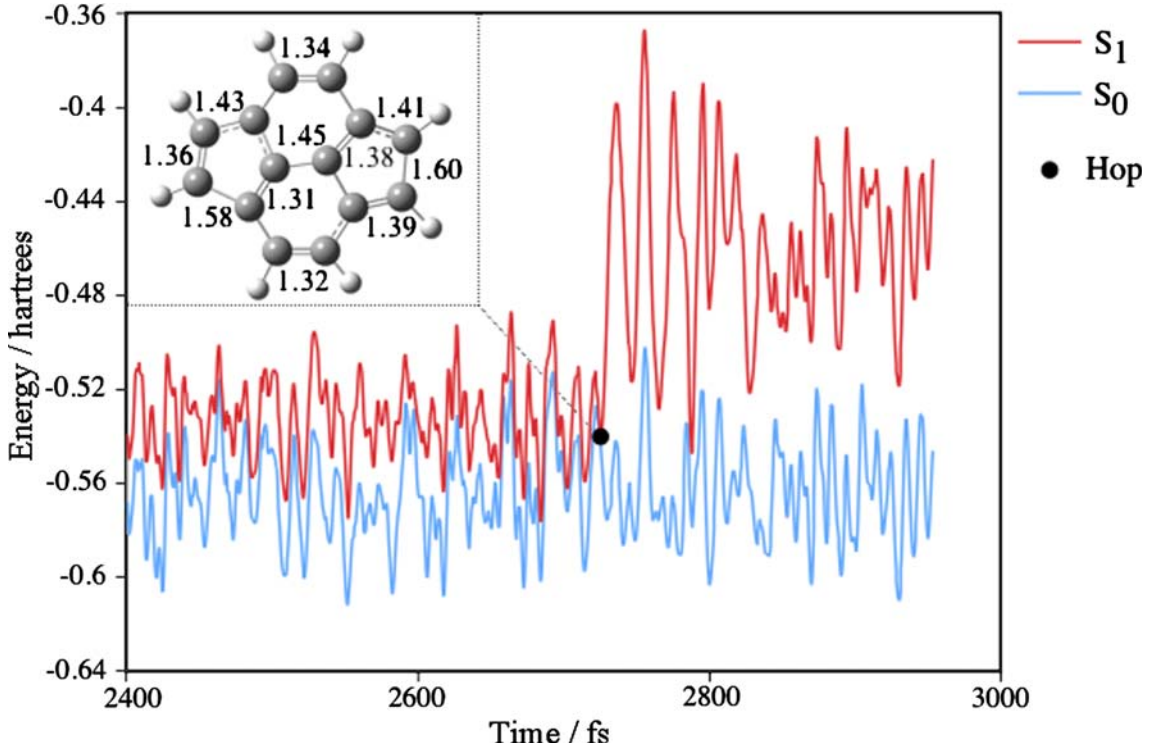

Fig. 7 A representative S_1 trajectory for pyracylene, showing that the geometry at which the hop to S_0 took place is similar to the C_{2h} crossing minimum (Fig. 4). All bond lengths in Å

geometry having very approximately the structure of the C_{2h} crossing minimum.

We have characterized two other structures for pyracylene using MMVB. Starting from the region of the C_{2h} intersection geometry on S_0, MMVB also locates a minimum corresponding to a second D_{2h} ground state isomer (Fig. 8, right). This second isomer is $\sim$15 kcal mol^{-1} above the first (Fig. 8, left = Fig. 4, left). We also find this higher-energy ground state isomer with RB3LYP (bond lengths agreeing with MMVB to within $\pm$0.01 Å), but it is unstable with respect to UB3LYP [68], and re-optimizing leads to an RB3LYP solution at the lower-energy $D_{2h}S_0$ minimum (Figs. 4, 8). With CASSCF, we could only obtain the $D_{2h}S_0$ minimum shown in Fig. 4: this does not appear to be a case of bistability, such as those investigated by Malrieu and Guihery [69], although the CASSCF gradient is small in the region of the higher-energy S_0 isomer (RMS gradient = 0.00039 a.u.).

We have also characterized a D_{2h} minimum on the S_2 surface of pyracylene. With MMVB, the vertical excitation energies to S_1 and S_2 are $\sim$4 kcal mol^{-1} apart. Relaxation on S_2 leads to the structure shown in Fig. 9, at which the S_2 and S_1 states are less than 1 kcal mol^{-1} apart, 31 kcal mol^{-1}

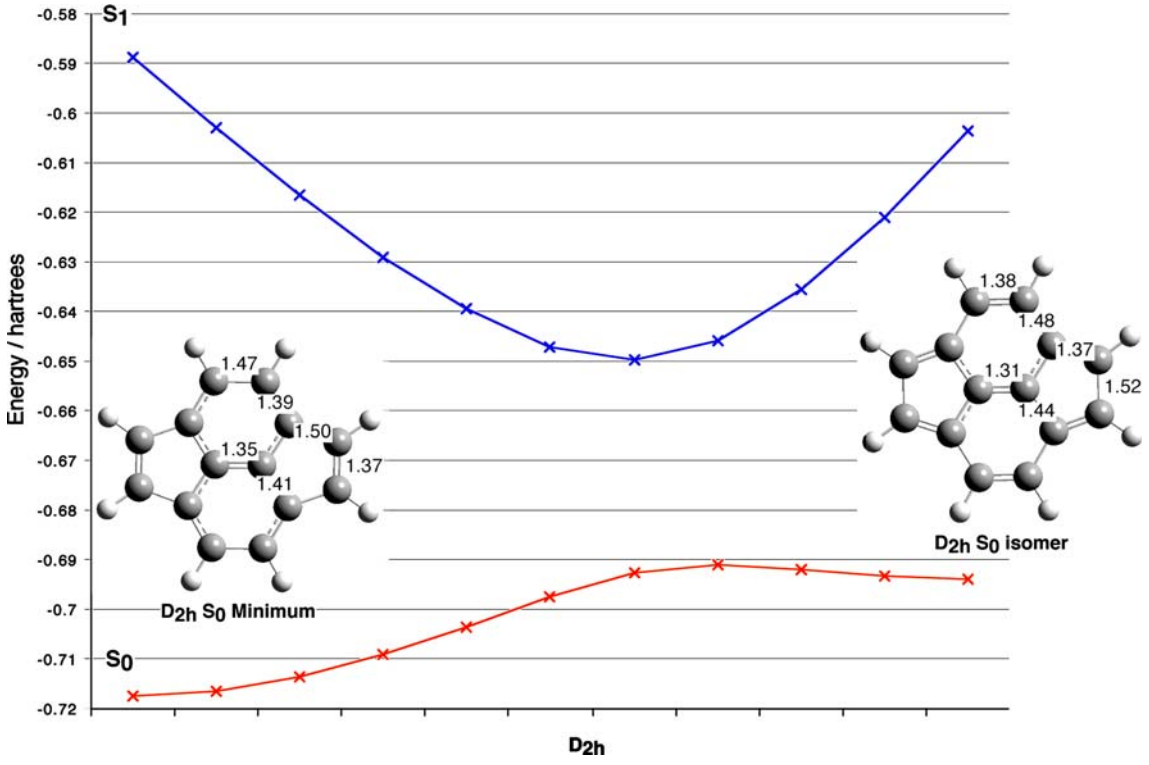

Fig. 8 Linear interpolation between the $D_{2h}S_0$ minimum and a higher-energy D_{2h} isomer on S_0 located with MMVB. All bond lengths in Å

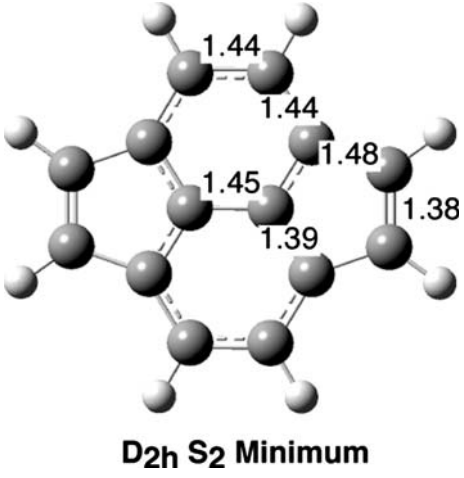

Fig. 9 The $D_{2h}S_2$ minimum of pyracylene calculated with MMVB. All bond lengths in Å

above the S_1 minimum. This S_2 state corresponds to an excitation of the naphthalene moiety [18]: the distinguishing feature of this structure is the long central C–C bond (1.45 Å; 0.1 Å longer than for the S_0 and S_1 minima). We mention this structure and the S_2 state for two reasons. Firstly, S_2 and S_1 'touch' but do not appear to cross with MMVB: the S_1 state that is vertically excited is the state that crosses with S_0 at the C_{2h} geometry shown in Fig. 4. Secondly, for systems such as pyracylene, there will in general be many excited states with minima at very different geometries, and small differences in their relative energies may lead to errors in the vertical order of the excited states and/or extra crossings and unexpected geometry changes. This is the main reason for comparing MMVB calculations with CASSCF/RASSCF.

As a test of the MMVB results, we used RASSCF to optimize the $C_{2h}S_1/S_0$ crossing, after calibrating RASSCF against CASSCF as described in the computational methods section. The RASSCF crossing (Fig. 10) is very similar to the MMVB one (bond lengths agree to within ± 0.02 Å), and the associated branching space vectors are also very similar. Moreover, we are confident that the RASSCF optimized geometry is a good approximation to the as-yet unattainable CASSCF geometry: we computed the CASSCF S_0–S_1 energy gap at the RASSCF optimized geometry, and the degeneracy is lifted by only 1.7 kcal mol^{-1}. It is worth noting that such a crossing would have been difficult to optimize without the initial MMVB guess for the geometry. Nonetheless, more ab initio calculations are needed on the excited states of pyracylene to validate the MMVB potential energy surfaces, as there appear to be several low-lying excited states in this system. Further comparison with CASSCF/RASSCF is currently in progress [90].

Finally, several authors have commented that the photophysical properties of polycyclic aromatic hydrocarbons containing 5-membered rings (abbreviated PCH5, CPAH, CP-PAH) are very different to those without (PAH), particularly the lack of fluorescence from S_1 [70–73], 'anomalous' emission from S_2 [74] and reduced resolution of vibrational

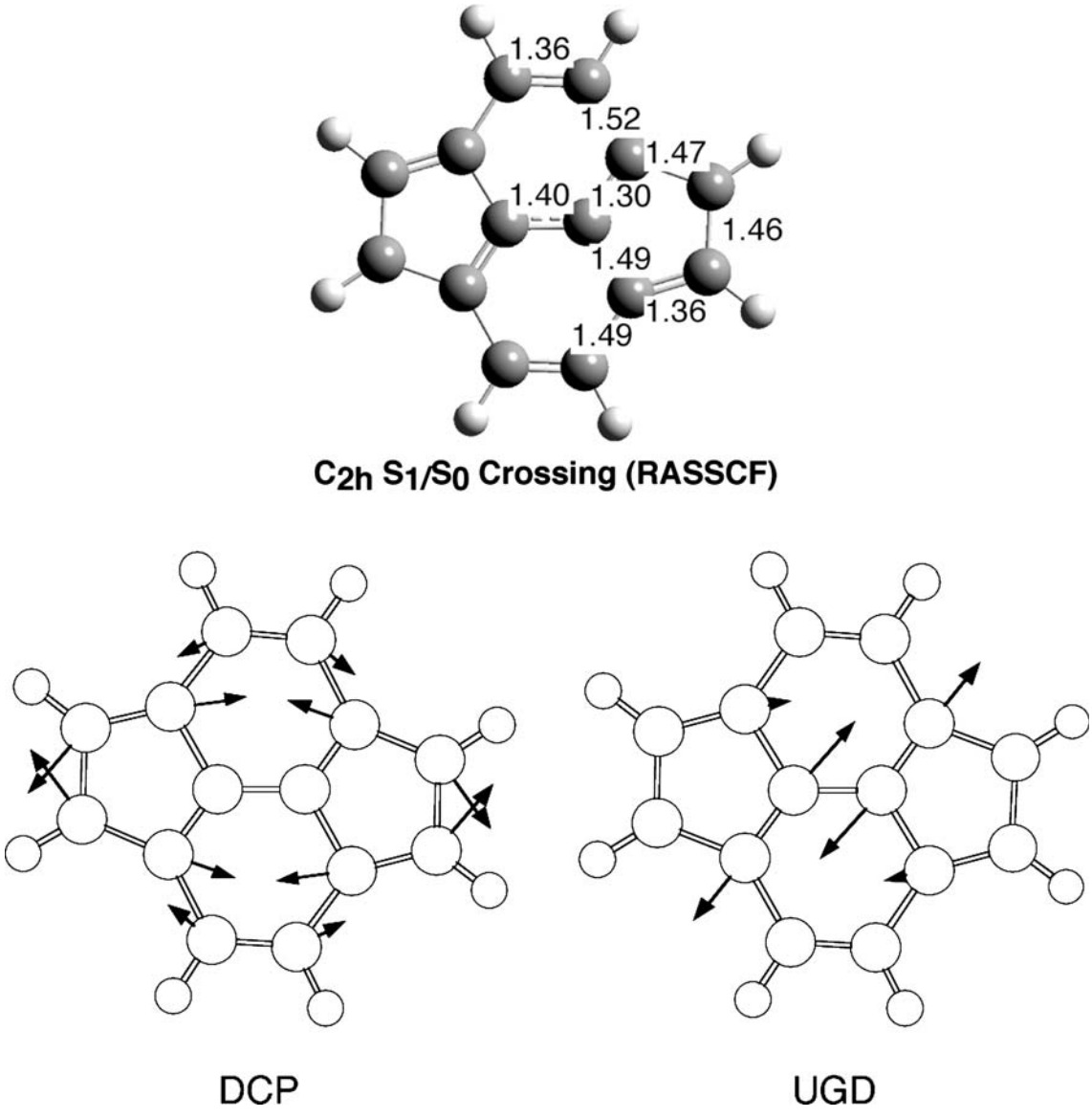

Fig. 10 The RASSCF optimized C_{2h} S_1/S_0 crossing geometry and associated DCP and UGD vectors. All bond lengths in Å

fine structure [75]. For example, cyclopenta[cd]-fluoranthene (two 5-membered rings) was found to be nonfluorescent, whereas fluoranthene itself (one 5-membered ring) is strongly fluorescent [73]. Cyclopenta[cd]fluoranthene is pyracylene with a benzene ring attached to one of the five membered rings, suggesting the existence of a similar low-lying S_1/S_0 conical intersection to pyracylene itself. We expect similar crossings to be found in other polycyclic aromatic hydrocarbons with two 5-membered rings. The key feature that will make these crossings accessible (as they are for azulene [22], fulvene [24,76] and pyracylene described here) is that the geometries needed to make the S_1 and S_0 states degenerate can all be achieved by small in-plane bond length adjustments. This contrasts with the out-of-plane distortions needed to obtain the degeneracy in benzene [21,67] and polyenes [35,77].

4 Results and discussion: DHA/VHF

The photochemical ring-opening reaction of DHA to give VHF (Fig. 3) is rapid and efficient, but VHF is photostable and does not react photochemically from the S_1 state to give DHA; the backward reaction only takes place thermally [50,51]. We have previously shown (using CASSCF calculations [52]) that all of these experimental observations can be explained by a conical intersection between S_1 and S_0 states. This crossing–reoptimised with MMVB–is shown in Fig. 11 (CI S_1/S_0). The minimum on the crossing has a geometry that is VHF-like, and is the lowest-energy point on S_1 overall (Table 2).

Figure 12a shows the DHA/VHF reaction coordinate (mainly a single bond being broken/formed) at the S_1 transition structure TS*, and Fig. 12b shows the degeneracy-lifting

Table 2 Molecular mechanics – valence bond energies for the DHA/VHF system (Fig. 11)

Geometry	S_0	S_1	$\Delta E(S_1–S_0)$	$\Delta E(S_0)$	$\Delta E(S_1)$
M S_0(DHA)	−0.72639	−0.51548	132.3	0.0	40.6
M S_1(DHA∗)	−0.69059	−0.58022	69.3	22.5	0.0
M S_0(VHF)	−0.67970	−0.52756	95.5	29.3	33.0
TS_1S_0	−0.61647	−0.55804	36.7	69.0	13.9
TS_2S_0	−0.63985	−0.59538	27.9	54.3	−9.5
$TS^* \times S_1$	−0.61204	−0.52140	56.9	71.7	36.9
CI S_1/S_0	−0.62851	−0.62851	<0.1	61.4	−30.3

Absolute energies in hartrees. ΔE in kcal mol^{-1}. $\Delta E(S_0)$ and $\Delta E(S_1)$ are calculated with the DHA S_0 and S_1 minimum energies respectively as references. TS_1 correspond to the DHA→VHF transition state on the ground state, whereas TS_2 correspond to a transition state on the VHF side perpendicular to the DHA→VHF reaction path. M minimum; TS transition structure; CI conical intersection

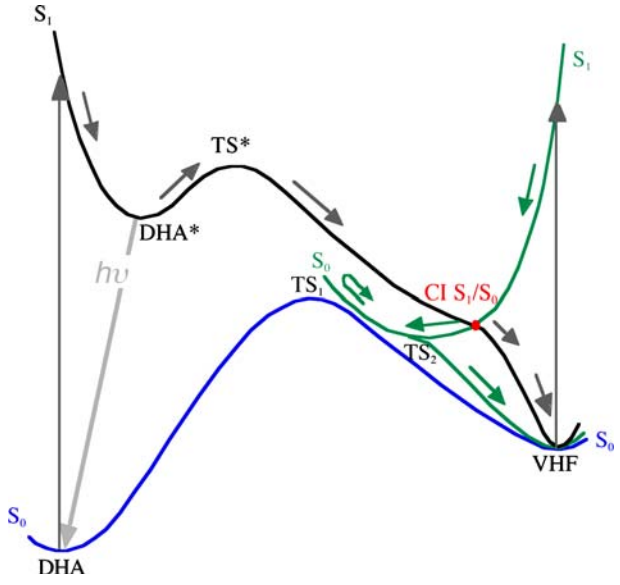

Fig. 11 The DHA/VHF MMVB critical points on the S_0 and S_1 potential energy surfaces. The *blue curve* indicates the ground state thermal reaction path. The *black and green curves* show the non-adiabatic DHA → VHF and VHF → VHF reaction pathways respectively.

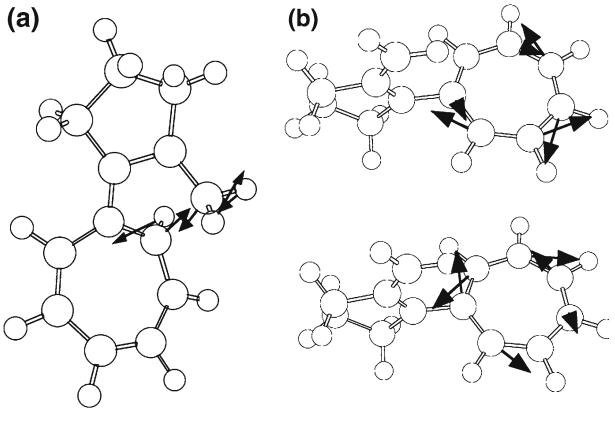

Fig. 12 The DHA/VHF **a** MMVB reaction coordinate (transition vector at the S_1 transition structure TS*, Fig. 11); **b** DCP and UGD vectors at the MMVB conical intersection

coordinates (mainly skeletal deformations of the heptafulvene ring) at the lowest-energy point of S_1/S_0 conical intersection. To a first approximation, the reaction coordinate at

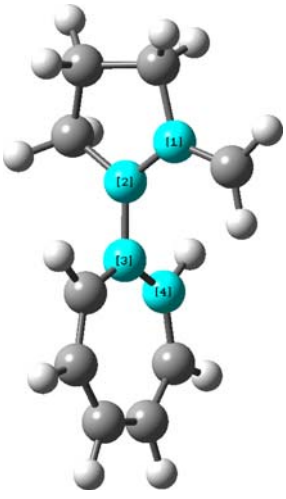

Fig. 13 The MMVB optimized S_1/S_0 conical intersection for DHA/VHF. Note that the crossing structure is twisted (dihedral angle 1–2–3–4 = 90°) and lies on the VHF side of the potential surface

TS* is independent of the branching space coordinates. For DHA, this means that decay to S_0 will most likely take place at the 'nearest' point on the S_1/S_0 crossing seam to TS*, and dynamics calculations are necessary (cf. diarylethylenes [40]). For VHF, almost the opposite is true: initial relaxation involves the skeletal deformations shown in Fig. 12b, and decay will take place in the region of the crossing minimum, but will not lead to ring closure along the coordinate shown in Fig. 12a, but back to the VHF S_0 minimum as shown on Fig. 11. VHF is therefore photostable, like pyracylene.

The MMVB topology of the DHA/VHF potential energy surfaces (Fig. 11) is similar to the CASSCF one [52]. However, some inaccuracies due to the approximate parameterization of MMVB were found. In particular, the optimized conical intersection at the MMVB level has a structure in which the two rings are orthogonal (Fig. 13). This is not the case with CASSCF. Therefore, the relaxation coordinate from VHF to CI S_1/S_0, which mainly involves skeletal deformations at the CASSCF level (one of the branching space coordinates), includes torsion as well at the MMVB level. Furthermore, the relative energies of DHA (closed) and VHF (open) are not well balanced in MMVB, because of problems with the MMVB parameters discussed in the computational methods section. For example, VHF was found

Table 3 Molecular mechanics–valence bond trajectories from DHA

Trajectory[a]	ΔE^{b}_{init}	ΔE^{c}_{hop}	$\Delta E(S_1–S_0)^{d}$	t^{e}_{hop}	t^{e}_{end}	ϕ^{f} (°)	Product[g]	E^{h}_{hop}
0	67.2	36.6	1.2	13.3	332.2	19	VHF	−0.57015
1	136.5	114.7	1.2	27.6	217.0	28	VHF	−0.44572
2	137.4	99.9	1.2	15.1	214.9	27	VHF	−0.46927
3	141.9	91.3	1.6	28.1	207.1	27	VHF	−0.48298
4	143.0	113.7	1.5	16.1	208.2	31	VHF	−0.44733
5	132.1	94.7	0.8	16.3	210.4	9	VHF	−0.47761
6	118.4	103.6	0.7	71.7	226.1	41	VHF	−0.46334
7	154.8	130.3	1.1	57.1	212.7	44	VHF	−0.42081
8	135.4	99.0	2.0	13.8	213.7	24	VHF	−0.47079
9	141.2	108.6	1.4	32.5	213.1	36	VHF	−0.45538

[a] See the computational details section
[b] Energy difference in kcal mol^{-1} between the electronic energy at the start of the trajectory and the degenerate electronic energy at the optimized conical intersection (Table 2)
[c] Energy difference in kcal mol^{-1} between the electronic energy at the hop and the degenerate electronic energy at the optimized conical intersection
[d] Energy gap in kcal mol^{-1} at the hop
[e] Time in femtoseconds at the hop, and at the end of the trajectory
[f] Dihedral angle measuring the twist between the two rings (Fig. 13)
[g] Final photoproduct formed
[h] Energy in hartrees of the S_1 state at the hop

Table 4 Molecular mechanics–valence bond trajectories from VHF

Trajectory[a]	ΔE^{b}_{init}	ΔE^{c}_{hop}	$\Delta E(S_1–S_0)^{d}$	t^{e}_{hop}	t^{e}_{end}	ϕ^{f} (°)	Product[g]	E^{h}_{hop}
0	63.3	14.7	1.6	5.1	340.9	14	VHF	−0.60515
1	123.3	90.7	2.8	53.0	228.5	23	VHF	−0.48400
2	126.5	83.0	1.3	68.9	229.0	23	VHF	−0.49626
3	113.5	84.3	2.5	37.8	225.0	28	VHF	−0.49420
4	115.2	89.6	3.0	4.5	222.1	6	VHF	−0.48571
5	97.4	78.1	2.0	150.2	244.3	47	VHF	−0.50406
6	100.3	80.6	2.8	21.1	116.7	21	VHF	−0.50004
7	142.1	99.8	0.9	108.3	225.5	27	VHF	−0.46940
8	112.9	69.5	2.7	149.3	242.4	62	VHF	−0.51778
9	148.6	69.8	2.6	110.2	222.0	23	VHF	−0.51730

[a] See the computational details section
[b] Energy difference in kcal mol^{-1} between the electronic energy at the start of the trajectory and the degenerate electronic energy at the optimized conical intersection (Table 2)
[c] Energy difference in kcal mol^{-1} between the electronic energy at the hop and the degenerate electronic energy at the optimized conical intersection
[d] Energy gap in kcal mol^{-1} at the hop
[e] Time in femtoseconds at the hop, and at the end of the trajectory
[f] Dihedral angle measuring the twist between the two rings (Fig. 13)
[g] Final photoproduct formed
[h] Energy in hartrees of the S_1 state at the hop

to be 29 kcal mol^{-1} higher in energy than DHA on S_0 with MMVB (Table 2), whereas it is only 4 kcal mol^{-1} higher at the CASSCF level.

Although accurate energetics are not so important for the study of the mechanism of DHA/VHF photochromism, the twisted configuration of the MMVB conical intersection minimum has some consequences for the dynamics. From DHA, the reaction path (Fig. 12a)–mainly involving a sigma bond breaking–is not included in the branching space (Fig. 12b). Therefore, the reference trajectory encounters the crossing seam at higher energy than the optimized crossing minimum (Table 3; note that the same behavior was observed at the CASSCF level [52]). For the DHA→VHF trajectories (Table 3), the system hits the crossing seam in all trajectories and decays to VHF (not DHA) in agreement with the experimental results. The system hits the seam very quickly (a few tens of fs) after leaving the S_1 transition state and at high energy (mean –0.46 ± 0.02 hartrees) compared to the crossing minimum (–0.629 hartrees) as expected. Decay occurs for torsion angle ϕ small compared to 90°, the optimized MMVB value for the crossing (Fig. 13).

From VHF, the MMVB reaction path is not fully included in the branching space either, since torsion is also necessary to reach the minimum on the crossing. Therefore, the reference trajectory from VHF on S_1 also hits the crossing seam at higher energy (mean –0.50 ± 0.02 hartrees) than the optimized crossing minimum (Table 4; note that this is a different behavior from CASSCF). For the VHF → VHF trajectories

(Table 4), the system hits the crossing seam in all trajectories and decays to VHF (which is photostable in agreement with the experimental results: no DHA is formed on the timescale of this simulation). As with DHA, decay occurs for torsion angle ϕ that is small compared to 90°, showing that this torsion is independent of the branching space coordinates that create and lift the degeneracy to first order. The mean energy for decay of VHF (from Table 4) is 25 kcal mol^{-1} lower than for DHA (from Table 3) as expected from Fig. 11: on average, different regions of the crossing seam are being sampled in each case, although the difference is not as great as would be obtained with CASSCF.

Overall, MMVB dynamics gives a good agreement with the experimental observations with high quantum yield for the photochemical ring-opening DHA → VHF reaction (the black curve in Fig. 11) and no photochemical ring-closure VHF → DHA reaction (the green curve in Fig. 11).

5 Conclusion

We developed the MMVB method following an original suggestion of Jean-Paul Malrieu and coworkers. By coupling a parameterized Heisenberg Hamiltonian to a standard classical force field (MM2), reliable ground and excited state geometries of conjugated hydrocarbons can be rapidly optimized. The MMVB method was central to our development of algorithms for locating conical intersections and calculating their associated decay dynamics as it is many orders of magnitude faster than CASSCF, provided that appropriate MMVB parameters are available.

As an example of locating a conical intersection, we have shown that there is an accessible conical intersection between the S_1 and S_0 states of pyracylene, which explains the experimentally observed photostability and rapid radiationless decay. RASSCF/CASSCF calculations support this MMVB result, but do not add anything new to the mechanism. We expect there to be similarly accessible crossings in other polycyclic aromatic hydrocarbons with two odd-membered rings, provided there are no other constraints.

As an example of the importance of dynamics for decay at a conical intersection, we show that the S_1 excited states of both dihydroazulene (DHA) and vinylheptafulvene (VHF) decay to give VHF, i.e. VHF is also photostable, like pyracylene. MMVB is useful for studying systems where the conical intersection is accessed indirectly by vibrations orthogonal to an excited state reaction path (such as DHA), as many trajectories need to be run to obtain a realistic mechanistic picture, and unlike pyracylene, a reaction path alone is insufficient.

Several current problems with MMVB have been described:

1. There is a tendency for molecules with fused 5-membered rings (such as pyracylene) to become non-planar. This is a delicate energy balance, as molecules such as corannulene $C_{20}H_{10}$ [78], a 5-membered ring in the middle of five 6-membered rings, are expected to be nonplanar.
2. There are problems with the VB parameters that describe the formation of new sigma bonds, leading to an exaggerated difference here between the energy of closed (DHA) and open (VHF) isomers, and also problems describing the twisted VHF conical intersection structure.
3. There is the possibility of spurious minima, such as the higher-energy $D_{2h}S_0$ isomer of pyracylene.

Further work will include: more RASSCF benchmarks for MMVB, particularly to investigate points (2) and (3) above, as one of the main limitations in further developing MMVB is the lack of excited state optimized geometries for extended conjugated hydrocarbons.

Acknowledgements Many thanks to Mike Frisch and Thom Vreven of Gaussian, Inc. and Imperial College London for supporting this work. Thanks also to Massimo Olivucci, who co-developed the first version of MMVB. We thank EPSRC (UK) for grant support including GR/F48029, GR/G03335, GR/H58070, and currently GR/S94704. We would also like to thank the EPSRC National Service for Computational Chemistry Software for granting us the computing resources to perform the MOLPRO calculations on pyracylene.

References

1. Malrieu JP (1981) Theor Chim Act 59:251
2. Malrieu JP, Nebot-Gil I, Sanchez-Marin J (1984) Pure App Chem 56:1241
3. Malrieu JP (1990) The Magnetic Description of Conjugated Hydrocarbons. In: Maksic ZB (ed) Theoretical models of chemical bonding, part 2: the concept of the chemical bond. Springer, Berlin Heidelberg New York, pp 107–136
4. Malrieu JP, Maynau D (1982) J Am Chem Soc 104:3021
5. Maynau D, Malrieu JP (1982) J Am Chem Soc 104:3029
6. Maynau D, Durand P, Daudey JP, Malrieu JP (1983) Phys Rev A 28:3193
7. Maynau D, Said M, Malrieu JP (1983) J Am Chem Soc 105:5244
8. Said M, Malrieu JP (1983) Chem Phys Lett 102:312
9. Said M, Maynau D, Malrieu JP, Garcia-Bach MA (1984) J Am Chem Soc 106:571
10. Said M, Maynau D, Malrieu JP (1984) J Am Chem Soc 106:580
11. Sanchez-Marin J, Malrieu JP (1985) J Phys Chem 89:978
12. Sanchez-Marin J, Malrieu JP (1985) J Am Chem Soc 107:1985
13. Treboux G (1994) J Phys Chem 98:10054
14. Treboux G, Maynau D, Malrieu JP (1995) J Phys Chem 99:6417
15. Durand P, Malrieu JP (1987) Adv Chem Phys 67:321
16. Bernardi F, Olivucci M, McDouall JJW, Robb MA (1988) J Chem Phys 89:6365
17. Bernardi F, Olivucci M, Robb MA (1992) J Am Chem Soc 114:1606
18. Bearpark MJ, Robb MA, Bernardi F, Olivucci M (1994) Chem Phys Lett 217:513
19. Bernardi F, Olivucci M, Ragazos IN, Robb MA (1992) J Am Chem Soc 114:8211
20. Bearpark MJ, Robb MA, Schlegel HB (1994) Chem Phys Lett 223:269–274
21. Smith BR, Bearpark MJ, Robb MA, Bernardi F, Olivucci M (1995) Chem Phys Lett 242:27
22. Bearpark MJ, Bernardi F, Clifford S, Olivucci M, Robb MA, Smith BR, Vreven T (1996) J Am Chem Soc 118:169
23. Bearpark MJ, Bernardi F, Olivucci M, Robb MA, Smith BR (1996) J Am Chem Soc 118:5254
24. Clifford S, Bearpark MJ, Bernardi F, Olivucci M, Robb MA, Smith BR (1996) J Am Chem Soc 118:7353
25. Bearpark MJ, Bernardi F, Olivucci M, Robb MA (1996) Int J Quant Chem 60:505

26. Bearpark MJ, Bernardi F, Olivucci M, Robb MA, Clifford S, Vreven T (1996) Mol Phys 89:37
27. Garavelli M, Celani P, Fato M, Bearpark MJ, Smith BR, Olivucci M, Robb MA (1997) J Phys Chem A 101:2023
28. Bearpark MJ, Bernardi F, Clifford S, Olivucci M, Robb MA, Vreven T (1997) J Phys Chem A 101:3841
29. Bearpark MJ, Bernardi F, Olivucci M, Robb MA, (1997) J Phys Chem A 101:8395
30. Deumal M, Bearpark MJ, Smith BR, Olivucci M, Bernardi F, Robb MA (1998) J Org Chem 63:4594
31. Klein S, Bearpark MJ, Smith BR, Robb MA, Olivucci M, Bernardi F (1998) Chem Phys Lett 292:259
32. Bearpark MJ, Celani P, Jolibois F, Olivucci M, Robb MA, Bernardi F (1999) Mol Phys 96:645
33. Bearpark MJ, Robb MA (2000) J Phys Chem A 104:1075
34. Jolibois F, Bearpark MJ, Klein S, Olivucci M, Robb MA (2000) J Am Chem Soc 122:5801
35. Garavelli M, Smith BR, Bearpark MJ, Bernardi F, Olivucci M, Robb MA (2000) J Am Chem Soc 122:5568
36. Robb MA, Bearpark MJ, Celani P, Bernardi F, Olivucci M (2000) Mol Cryst Liq Cryst 344:31–39
37. Garavelli M, Bernardi F, Olivucci M, Bearpark MJ, Klein S, Robb MA (2001) J Phys Chem A 105:11496
38. Garavelli M, Ruggeri F, Ogliaro F, Bearpark MJ, Bernardi F, Olivucci M, MA Robb (2002) J Comp Chem 24:1357
39. Bearpark MJ, Boggio-Pasqua M (2003) Theor Chem Acc 110:105
40. Boggio-Pasqua M, Ravaglia M, Bearpark MJ, Garavelli M, Robb MA (2003) J Phys Chem A 107:11139
41. Frisch MJ, Trucks GW, Schlegel HB, Scuseria GE, Robb MA, Cheeseman JR, Montgomery JA, Vreven T, Kudinv, Burant JC, Millam JM, Iyengar SS, Tomasi J, Barone V, Mennucci B, Cossi M, Scalmani G, Rega N, Petersson GA, Nakatsuji H, Hada M, Ehara M, Toyota K, Fukuda R, Hasegawa J, Ishida M, Nakajima T, Honda Y, Kitao O, Nakai H, Klene M, Li X, Knox JE, Hratchian HP, Cross JB, Adamo C, Jaramillo J, Gomperts R, Stratmann RE, Yazyev O, Austin AJ, Cammi R, Pomelli C, Ochterski JW, Ayala PY, Morokuma K, Voth GA, Salvador P, Dannenberg JJ, Zakrzewski VG, Dapprich S, Daniels AD, Strain MC, Farkas O, Malick DK, Rabuck AD, Raghavachari K, Foresman JB, Ortiz JV, Cui Q, Baboul AG, Clifford S, Cioslowski J, Stefanov BB, Liu G, Liashenko A, Piskorz P, Komaromi I, Martin RL, Fox DJ, Keith T, Al-Laham MA, Peng CY, Nanayakkara A, Challacombe M, Gill PMW, Johnson B, Chen W, Wong MW, Gonzalez C, Pople JA (2003) Gaussian Development Version, Revision B.07, Gaussian, Inc., Pittsburgh PA
42. Blancafort L, Celani P, Bearpark MJ, Robb MA, (2003) Theor Chem Acc 110:92
43. Allinger NL (1976) Adv Phys Org Chem 13:1
44. Boggio-Pasqua M, Bearpark MJ, Klene M, Robb MA (2004) J Chem Phys 120:7849
45. Turro NJ (1978) Modern Molecular Photochemistry, Benjamin/Cummings, Menlo Park, pp 147–148
46. Atchity GJ, Xantheas SS, Ruedenberg K (1991) J Chem Phys 95:1862
47. Freiermuth B, Gerber S, Riesen A, Wirz J, Zehnder M (1990) J Am Chem Soc 112:738
48. Malrieu JP (1998) J Mol Struct Theochem 424:83
49. Salem L (1966) The molecular orbital theory of conjugated systems. Benjamin, New York
50. Daub J, Knochel T, Mannschreck A (1984) Angew Chem Int Ed Eng 23:960
51. Ern J, Petermann M, Mrozek T, Daub J, Kuldova K, Kryschi C, (2000) Chem Phys 259:331
52. Boggio-Pasqua M, Bearpark MJ, Hunt PA, Robb MA (2002) J Am Chem Soc 124:1456
53. Yarkony DR (1998) Acc Chem Res 31:511
54. Groenhof G, Bouxin-Cademartory M, Hess B, De Visser SP, Berendsen HJC, Olivucci M, Mark AE, Robb MA (2004) J Am Chem Soc 126:4228
55. Weingart O, Migani A, Olivucci M, Robb MA, Buss V, Hunt P (2004) J Phys Chem A 108:4685
56. Heitler W, London F (1927) Z Phys 44:455
57. Helgaker T, Uggerud E, Jensen HJA (1990) Chem Phys Lett 173:145
58. Chen W, Hase WL, Schlegel HB (1994) Chem Phys Lett 228:436
59. Preston, RK, Tully, JC (1971) J Chem Phys 54:4297
60. Preston, RK, Tully, JC (1971) J Chem Phys 55:562
61. Blancafort L, Ogliaro F, Olivucci M, Robb MA, Bearpark MJ, Sinicropi A (2005) In: Kutateladze A (ed) Computational methods in photochemistry, chap 2. Dekker/CRC, Boca Raton
62. Werner H-J, Knowles PJ, Amos RD, Bernhardsson A, Berning A, Celani P, Cooper DL, Deegan MJO, Dobbyn AJ, Eckert F, Hampel C, Hetzer G, Korona T, Lindh R, Lloyd AW, McNicholas SJ, Manby FR, Meyer W, Mura ME, Nicklass A, Palmieri P, Pitzer R, Rauhut G, Schütz M, Schumann U, Stoll H, Stone AJ, Tarroni R, Thorsteinsson T (2002) MOLPRO
63. Diogo HP, Kiyobayashi T, da Piedade MEM, Burlak N, Rogers DW, McMasters D, Persy G, Wirz J, Liebman JF (2002) J Am Chem Soc 124:2065
64. Bird CW (1998) Tetrahedron 54: 10179. Pyracylene S_0 calculated with MMVB looks like structure 11b in this paper; S_1 is like 11c.
65. Gerhartz W, Poshusta RD, Michl J (1977) J Am Chem Soc 99:4263
66. Gerhartz W, Poshusta RD, Michl J (1976) J Am Chem Soc 98:6427
67. Palmer IJ, Ragazos IN, Bernardi F, Olivucci M, Robb MA (1993) J Am Chem Soc 115:673
68. Pople JA, Gill PMW, Handy NC (1995) Int J Quant Chem 56:303
69. Guihery N, Malrieu JP, Maynau D, Handrick K (1997) Int J Quant Chem 61:45
70. Schael F, Lohmannsroben HG (1992) J Photochem Photobiol A 69:27
71. Dunsbach R, Schmidt R (1994) J Photochem Photobiol A 83:7
72. Sarobe M, Flink S, Jenneskens LW, Vanpoecke BLA, Zwikker JW (1995) J Chem Soc Chem Comm (23):2415–2416
73. Sarobe M, Snoeijer JD, Jenneskens LW, Slagt MQ, Zwikker JW (1995) Tet Lett 36:8489
74. Gooijer C, Kozin I, Velthorst NH, Sarobe M, Jenneskens LW, Vlietstra EJ (1998) Spectrochim Acta A 54:1443
75. Marsh ND, Mikolajczak CJ, Wornat MJ (2000) Spectrochim Acta A 56:1499
76. Paterson MJ, Bearpark MJ, Robb MA, Blancafort L (2004) J Chem Phys 121:11562
77. Garavelli M, Bernardi F, Celani P, Robb MA, Olivucci M (1998) J Photochem Photobiol A Chem 114:109
78. Fawcett JK, Trotter J (1966) Proc R Soc A 289:366
79. Toniolo A, Olsen S, Manohar L, Martinez TJ (2004) Faraday Discussions 127:149
80. Toniolo A, Thompson AL, Martinez TJ (2004) Chem Phys 304:133
81. Toniolo A, Ciminelli C, Granucci G, Laino T, Persico M (2004) Theor Chem Acc 111:270
82. Sulpizi M, Rohrig UF, Hutter J, Rothlisberger U (2005) Int J Quant Chem 101:671
83. Ferre N, Cembran A, Garavelli M, Olivucci M (2004) Theor Chem Acc 112:335
84. Vreven T, Morokuma K (2003) Theor Chem Acc 109:125
85. Jasper AW, Zhu CY, Nangia S, Truhlar DG (2004) Faraday Discussions 127:1
86. Blancafort L, Hunt P, Robb MA (2005) J Am Chem Soc 127:3391
87. Hack MD, Wensmann AM, Truhlar DG, Ben-Nun M, Martinez TJ (2001) J Chem Phys 115:1172
88. Ben-Nun M, Quenneville J, Martinez TJ (2000) J Phys Chem A 104:5161
89. Worth GA, Robb MA, Burghardt I (2004) Faraday Discussions 127:307
90. Boggio–Pasqua M, Robb MA, Bearpark MJ (2005) J Phys Chem A 109:8849-8856